Nanoscale

PAPER

Check for updates

Titania (TiO₂) nanotube surfaces doped with zinc and strontium for improved cell compatibility

Abhishek Bhattacharjee,[a] Bruno Pereira,[b] Paulo Soares[b] and Ketul C. Popat ⓘ *[a,c,d,e]

Titanium-based orthopedic implants are gaining popularity in recent years due to their excellent bio-compatibility, superior corrosion resistance and lightweight properties. However, these implants often fail to perform effectively due to poor osseointegration. Nanosurface modification approaches may help to resolve this problem. In this work, TiO₂ nanotube (NT) arrays were fabricated on commercially available pure tita-nium (Ti) surfaces by anodization and annealing. Then, zinc (Zn) and strontium (Sr), important for cell signal-ing, were doped on the NT surface by hydrothermal treatment. This very simple method of Zn and Sr doping takes less time and energy compared to other complicated techniques. Different surface characterization tools such as scanning electron microscopy (SEM), X-ray photoelectron spectroscopy (XPS), energy-dispersive X-ray spectroscopy (EDS), static water contact angle, X-ray diffraction (XRD) and nanoindentation techniques were used to evaluate the modified surfaces. Then, adipose derived stem cells (ADSCs) were cul-tured with the surfaces to evaluate cell adhesion, proliferation, and growth on the surfaces. After that, the cells were differentiated towards osteogenic lineage to evaluate alkaline phosphatase (ALP) activity, osteocal-cin expression, and calcium phosphate mineralization. Results indicate that NT surfaces doped with Zn and Sr had significantly enhanced ADSC adhesion, proliferation, growth, and osteogenic differentiation com-pared to an unmodified surface, thus confirming the enhanced performance of these surfaces.

Introduction

Orthopedic implants play a key role to provide necessary support to the dynamic bone tissue while it undergoes remo-deling and healing at the damaged site.[1] For a successful bone healing, interaction between the implant surface and bone tissue is profoundly important and determines the success of the bone healing process. A proper interaction between the implant and bone tissue by the formation of new bone matrix around the implant is known as osseointegra-tion.[2] An adequate osseointegration is determined by the osteoblast differentiation of mesenchymal stem cells (MSC) which is known as osteoinductivity, along with the new bone matrix deposition on the material surface known as osteoconductivity.[3,4] Therefore, the osteoblast differentiation on the implant surface can be a good indicator to understand the efficacy of the implant for better osseointegration. For

that reason, it is imperative to design implant surfaces that promote good osseointegration resulting in successful bone healing.

Orthopedic implants can be made of different materials such as metallic, polymeric, ceramic or composites. For example, a polymeric implant can be used for healing a damaged soft cartilage tissue. However, when the goal is to provide robust support to the damaged bone, a metallic implant is a better choice over polymer due to high cyclic load bearing capacity of metals over polymers. Certain reasons dictate the dominance of metals as orthopedic implants, one of which is the chemical inertness offered by the presence of an oxide layer on passive metal surfaces.[5] Since 1921, the three most popular choices of metallic orthopedic implants were stainless steel (SS), chromium–cobalt (CC) alloys, and titanium (Ti) based implants.[5] Among these choices, Ti offers superior advantage over the others owing to its corrosion prevention, inertness, superior strength, and lightweight properties.[6] Additionally, Ti possesses excellent biocompatibility that helps in reducing immune response and bacterial infection after the orthopedic implant surgery. However, around 10% of Ti based implants fail each year mainly due to poor osseointegration which causes aseptic loosening of the implant from the desired bone site.[4]

To improve the osseointegration properties of the Ti implants, nanosurface modification approaches have been uti-

[a]School of Advanced Materials Discovery, Colorado State University, Fort Collins, CO, USA; Department of Bioengineering, George Mason University, Fairfax, VA, USA. E-mail: ketul.popat@colostate.edu
[b]Department of Mechanical Engineering, Pontifícia Universidade Católica do Paraná, PR, Brazil
[c]Mechanical Engineering, Colorado State University, Fort Collins, CO, USA
[d]School of Biomedical Engineering, Colorado State University, Fort Collins, CO, USA
[e]Department of Bioengineering, George Mason University, Fairfax, VA, USA

lized in recent years. Introduction of nanoscale features on pure Ti surface were found to increase extracellular matrix protein absorption and cell attachment, while stimulating the osteogenic differentiation.[7] Several nano and micro surface modifications on Ti surfaces have been utilized in recent years.[8] Among them, nanotube structures are interesting because they impart additional material properties such as wettability, mechanical flexibility, hemocompatibility, and biocompatibility which are advantageous over pure Ti.[9,10] The nanotubes are formed by continuous anodization and etching of the TiO_2 layer. One of the important advantages of the nanotube structure is that they can act as anchoring points for the MSCs to adhere efficiently to the surface. Another advantage is that the nanotube structures are flexible in nature and help in accommodating the mechanical stress coming from the cells which results in better cell attachment and spread. There have been reports of further modifying the titania nanotube surfaces to implement better cell compatibility and osteogenic properties for implant applications. One such example is the incorporation of antimicrobial peptides (AMPs) on the nanotubes that helped in achieving excellent antibacterial properties.[11] However, they do not provide any relevant important signaling elements to the cells to differentiate into a specific phenotype. Therefore, a new approach should be investigated for nanosurface modification of Ti to improve the osseointegration properties.

Zinc (Zn) and strontium (Sr) act as important signaling elements for the MSCs to differentiate into osteoblasts. Zn is found as a micronutrient in bone and help in bone formation.[12,13] Additionally, previous studies reported that Zn provides antibacterial activity to the surfaces.[14–16] On the other hand, Sr is another important trace element for maintaining bone health. Sr helps in reducing osteoclast formation and improves osteoblasts differentiation which helps in bone healing instead of bone resorption.[17,18] For these reasons, incorporation of these important trace elements on the implant surface may help in achieving better cell compatibility and osseointegration. Different doping techniques such as hydrothermal, alkaline heat-treatment, photo electrolytic oxidation (PEO), micro-spark oxidation, magnetron sputtering, and plasma spray have been reported in the literature.[19] Among these methods, hydrothermal process is relatively simple since it uses only few chemicals and a lower reaction time. In a previous study, Zn was doped on Ti surfaces using hydrothermal and alkaline-heat treatment, and it was found that hydrothermally treated surfaces provided better antibacterial activity than the alkaline-heat treated surfaces.[20] In this study, Zn and Sr, were doped on the titanium surfaces *via* hydrothermal treatment. The surfaces were characterized by using scanning electron microscopy (SEM), X-ray photoelectron spectroscopy (XPS), and energy dispersive spectroscopy (EDS) to understand surface morphology along with concentration and distribution of Zn and Sr on the surfaces. Static water contact angle was measured using a goniometer to understand the surface wettability. X-ray diffraction (XRD), nanoindentation hardness (H) and elastic modulus (E) were also measured to understand surface crystallinity and mechanical properties of the surfaces. Then cell compatibility of these surfaces was evaluated using adipose derived stem cells (ADSCs). Since ADSCs are MSCs derived from the abundant adipose tissue by minimally invasive procedure, their use is gaining popularity for biomaterials research.[21] ADSC adhesion, proliferation, and differentiation to osteoblastic phenotype was analyzed on different surfaces. After that, adhered ADSCs were differentiated towards osteoblastic lineage. After 1 and 3 weeks of ADSC culture, alkaline phosphatase (ALP) activity, osteocalcin expression, and cell mineralization were analyzed to evaluate ADSC differentiation towards osteoblasts on the modified surfaces. The results indicate that surfaces with Zn and Sr could significantly improve ADSC adhesion and proliferation compared to pure titanium. TiO_2 nanotube (NT) surface doped with Sr exhibited the most promising result by enhanced ADSC differentiation towards osteoblasts compare to other surfaces indicating its potential of being used as an effective orthopedic implant surface.

Experimental methods

Titania nanotube surface fabrication

To fabricate titania (TiO_2) nanotube arrays on commercially available pure titanium (Ti) surface, a method described in a previous work was followed.[6] Briefly, titanium surfaces of 2 cm × 2 cm were cut and polished using silicon carbide sheets. Then they were soaked for 3 min in acetone followed by 10 min of sonication using a bath sonicator. Then the surfaces were cleaned using soap and isopropyl alcohol followed by 10 min of sonication in isopropyl alcohol and deionized (DI) water respectively. Then the surfaces were dried inside the fume hood prior to anodization. For anodization, an electrolyte solution containing 95% diethylene glycol (DEG, Thermo Fisher Scientific Chemicals Inc., Ward Hill, MA, USA), 2% hydrofluoric acid (HF, 48%, KMG Electronic Chemicals, Inc., Houston, TX, USA), and 3% DI water was prepared. Then cleaned Ti surfaces were connected to the electrolytic cell as anode using alligator tips. Similar sized platinum (Pt) surfaces were connected to the electrolytic cell as cathode. Then 55 kV electricity was applied to the electrolytic cells for 22 h at room temperature to perform anodizing and electrochemical etching on the Ti surfaces resulting in fabrication of nanotube arrays. After anodization, the surfaces were thoroughly cleaned with DI water and isopropyl alcohol and dried inside a hood for further processing. A control group of surfaces were annealed right after anodization at 530 °C for 3 h with 15 °C min^{-1} temperature increments. These surfaces were designated as NT. Cleaned Ti surfaces were also used as controls.

Zinc and strontium doping on different surfaces

Zinc (Zn) and strontium (Sr) were doped on anodized titanium surfaces by hydrothermal treatment. For Zn doping, the surfaces were incubated with a solution of 0.1 M zinc acetate inside a polytetrafluoroethylene (PTFE) lined hydrothermal

autoclave reactor for 1 h at 200 °C. To dope Sr, the surfaces were incubated with a solution of 0.02 M strontium acetate octahydrate inside a polytetrafluoroethylene (PTFE) lined hydrothermal autoclave reactor for 1 h at 200 °C. After the treatment, the surfaces were cleaned thoroughly with running DI water to remove excess solution. Finally, the surfaces were annealed at 530 °C for 3 h inside a furnace to prepare NTZn and NTSr surfaces.

Surface characterization

Different surface properties such as surface morphology, Zn and Sr distribution on the surface, surface chemistry, stability, wettability, and mechanical properties were evaluated in this work. These different surface characterization methodologies are described below.

• To characterize the morphology of Ti, NT, NTZn, and NTSr surfaces, scanning electron microscopic (SEM) images were collected using a JEOL JSM-6500F field emission scanning electron microscope (FESEM). The operating voltage was 15 kV with a probe current of 7 A. SEM images were collected in varying magnifications from 500× to 30 000×. To ensure high-equality SEM images, working distance, contrast and brightness were adjusted during the image collection process.

• To examine the surface chemistry, X-ray photoelectron spectroscopy (XPS) survey spectra were collected for each surface. A PHI Physical Electronics PE-5800 X-ray Photoelectron Spectrometer with an Al Kα X-ray source was used to collect the survey spectra from 0 V to 1100 V. MultiPak (version 9.6.1.7) software was used to analyze the XPS spectra. From the survey spectra, corresponding atomic weight percentage (% at) of each element on the surfaces were analyzed using the MultiPak software.

• To confirm a uniform distribution of Zn and Sr on the surfaces, energy-dispersive X-ray spectroscopy (EDS) was used. An Oxford SDD EDS detector connected to the FESEM was utilized to collect the EDS spectra and corresponding element maps for each surface. Oxford Aztec software was used to analyze the EDS spectra and maps.

• To evaluate wettability of the surfaces, static water contact angle was measured using a Ramé-Hart goniometer (Ramé-Hart Instrument Co., Succasunna, NJ, USA). A DI water droplet of approximately 10 μl was dropped on each surface using a micrometer syringe. An image of the droplet was collected using the camera system of the goniometer. Finally, contact angle values were measured from the images using the DROPimage software.

• To examine surface crystallinity, X-ray diffraction (XRD) spectra were collected using XRD-7000 Shimadzu. CuKα radiation at 40 kV and 30 mA was utilized while collecting the spectra. A thin film geometry with an incidence angle of 5° was used. Continuous scans from 20° to 80° at a scanning speed of 1° min^{-1} was used to collect the diffractograms. Match! software with PDF2 database was used for indexing the peaks.

• Surface mechanical properties such nanoindentation hardness (H) and elastic modulus (E) were evaluated by using a nanoindentation procedure. A Nanoindenter (ZwicK-Roell/Asmec) was programmed by an array (5 × 5), with 50 μm distance between each indentation and 0.1 N of maximum applied force on the surface by a calibrated Berkovich tip. The indentation method used was the quasi-continuous stiffness measurement (QCSM) method. This method allows for high accuracy measurements due to a progressively increasing force (from 0–100 mN for this study) combined with a dwell time at each force point.

• To evaluate the Zn and Sr stability on the surfaces, XPS spectra of each surface was collected at 0 and 28 days of incubation with DI water. 1 cm × 1 cm surfaces were cut and XPS spectra were taken at 0 day. From the spectra, atomic weight% (at%) of the respective Zn and Sr were calculated. Then, the surfaces were incubated with 500 ml of DI water for 28 days. XPS spectra were collected again and at% were calculated to evaluate the change in Zn and Sr concentration on the surfaces.

Adipose derived stem cell (ADSC) culture

Adipose derived stem cells (ADSCs) of passage 3 were generously donated by Dr Kimberly Cox-York from the Department of Food Science and Human Nutrition at the Colorado State University. The ADSCs were cultured in a growth medium containing 90% MEM Alpha Modification (1×, cytiva, Marlborough, MA, USA), 9% fetal bovine serum (FBS), and 1% penicillin–streptomycin in an incubator at 37 °C and 5% CO$_2$. Prior to the cell compatibility studies, surfaces of 1 cm × 1 cm dimensions were cut and sterilized with 70% ethanol and then thoroughly cleaned with DI water and PBS followed by further sterilization with UV light for 30 min inside a biological safety hood. Then the surfaces were taken into 48-well plates and 20 000 ADSCs per well were introduced. Then the well plates were incubated at 37 °C and 5% CO$_2$ for subsequent experiments. The growth media was changed after 4 days of incubation for all the well plates.

Cytotoxicity evaluation

To evaluate the cytotoxicity of the surfaces, a lactate dehydrogenase (LDH) based indicator assay (CyQuant™ LDH Cytotoxicity Assay Kit, ThermoFisher Scientific, Waltham, MA, USA) was used. ADSCs (passage 6) were cultured separately followed by the method described above. Then, the surfaces were sterilized and incubated with 20 000 ADSCs per well for 24 h. After the incubation, 90 μl supernatant from each well were collected in a sterile 90 well plate. Then, manufacturer's protocol was followed to determine the cytotoxicity of the surfaces.

Cell adhesion, proliferation, and morphology on the surfaces

• To evaluate cell adhesion and proliferation on the surfaces, the surfaces were taken out from the incubator after 4 and 7 days. The surfaces were then rinsed with PBS for 3 times to remove any unadhered cells. Then adhered cells were fixed on the surfaces using 3.7% formaldehyde in PBS for 15 min followed by 3 rinses with PBS. The fixed cells were then permealized using 1% Triton-X in PBS followed by two rinses with

PBS. Then the surfaces were incubated for 25 min in 70 nM rhodamine phalloidin (Cytoskeleton, Inc., Denver, CO, USA) which stained the actin filaments of the cells. Then 300 nm nuclear stain DAPI (ThermoFisher Scientific, Waltham, MA, USA) was added. Then the surfaces were incubated for 5 min followed by 2 rinses with PBS. Finally, a fluorescence microscope (Zeiss) was used to collect images of the surfaces. The images were analyzed to quantify cell adhesion and proliferation by counting the number of stained nuclei (DAPI) using imageJ software.

• SEM images were collected to examine the adhered cell morphology on the surfaces. Prior to image collection, the surfaces were taken out from the incubator after 4 and 7 days of incubation. Then the surfaces were rinsed 3 times with PBS to remove any unadhered cells. Then the surfaces were incubated with a primary fixative solution containing 3% glutaraldehyde (Sigma-Aldrich, St Louis, MO, USA), 0.1 M sucrose (Sigma-Aldrich, St Louis, MO, USA), and 0.1 M sodium cacodylate (Electron Microscopy Sciences, Hatfield, PA, USA) in DI water for 45 min at room temperature. After that, the surfaces were incubated with a buffer solution containing the primary fixative without the glutaraldehyde for 10 min. Then the adhered cells were dehydrated using 35%, 50%, 75%, and 100% sequentially for 10 min in each solution. Then the surfaces were gold coated (10 nm thickness) using a sputter coater to enhance the conductivity of the adhered cells. Finally, the FESEM was used to take images of the surfaces at 15 kV with 7 A probe current. Images of different magnifications ranging from 100× to 2000× were collected. Brightness, contrast, and working distance settings were adjusted for ensuring high-quality of the SEM images.

Osteogenic differentiation of ADSCs

After 7 days of ADSC culture with the growth media, osteogenesis was introduced using an osteogenic differentiation media. This media was prepared by taking the growth media and supplementing it with 10^{-8} M dexamethasone (Sigma, 98%), 50 µg mL^{-1} ascorbic acid (Sigma, 100%), and 6 mM β-glycerol phosphate (Sigma, 98%). The differentiation media was changed every other day for all the surfaces for 3 weeks. After 1 and 3 weeks of incubation period, the surfaces were analyzed to evaluate cell differentiation properties.

• Alkaline phosphate (ALP) activity of the cells at 1 and 3 weeks normalized by total protein content was evaluated to determine the differentiation activity of ADSCs when incubated with the surfaces. QuantiChrom™ Alkaline Phosphatase Assay Kit (DALP-250) (BioAssay Systems, Hayward, CA) was used for colorimetric determination of serum alkaline phosphatase activity. To measure the total protein content, a Micro BCA Protein Assay Kit (ThermoFisher Scientific, Waltham, MA, USA) was used. Manufacturer's protocols were followed to collect and analyze data for both assays.

• Immunofluorescence (IF) images were collected for all the surfaces to evaluate osteocalcin expression from the differentiated osteoblasts. For this, the surfaces were collected after 1 and 3 weeks, and washed with PBS for 3 times. Then the

cells were fixed using 3.7% formaldehyde in PBS for 15 min followed by 3 rinses with PBS. The fixed cells were then permealized using 1% Triton-X in PBS followed by two rinses with PBS. After that, the cells were incubated with a blocking serum in PBS for 30 min followed by a rinse with PBS. Then, the surfaces were incubated with a primary osteocalcin antibody solution (1 : 100 in 1% BSA) for 1 h followed by three rinses with PBS. After that, the surfaces were incubated with a secondary FITC-conjugated antibody (1 : 200 in 1% BSA) for 45 min followed by two PBS rinses. After that, actin filament stain rhodamine phalloidin and nuclear stain DAPI were added followed by the procedure described above. Finally, IF images of the surfaces were collected using a fluorescence microscope (Zeiss). Osteocalcin coverage area and the number of adhered cells were analyzed from the images using imageJ software.

• SEM images were also collected to determine hydroxyapatite (HA) mineral deposition by differentiated osteoblasts. After 1 and 3 weeks of incubation, the surfaces were washed with PBS 3 times and the adhered cells were fixed to the surfaces following the SEM protocol described above. EDS elemental maps were also collected to confirm the elemental composition of the deposited minerals.

Statistical analysis

For morphological surface characterization via SEM, at least 5 images were taken for each sample group ($n_{min} = 5$). For XPS, EDS, surface wettability analysis, 3 samples were used for each sample group ($n_{min} = 3$). During cell study, 3 samples were used for taking 9 fluorescence microscope images ($n_{min} = 9$). For cell viability, cytotoxicity, and protein studies (ALP, BCA) at least 4 samples were used for each sample group ($n_{min} = 4$). To evaluate statistically significant difference between sample groups, analysis of variance (ANOVA) was conducted followed by post-hoc T-test ($α = 0.05$).

Results and discussion

Surface characteristics of materials dictates the way a biological agent such as bacteria or cell interacts with the material. Previous studies suggest that nanoscale surface features can help in reducing bacterial infection along with increment in stem cell adhesion, proliferation, and differentiation.[8,22–24] Therefore, several material characterization techniques were utilized in the current study to understand the surface features of the modified Ti surfaces. First, morphological features of the surfaces were evaluated with scanning electron microscopic (SEM) images (Fig. 1). Ti had relatively smooth morphology with no unique distinguishable features. When TiO$_2$ nanotubes (NT) were formed on the Ti surfaces via anodization and annealing, significant morphological change was observed. When Ti surfaces is used as anode in an electrolyte solution containing hydrofluoric acid (HF) alongside platinum as cathode, two separate processes happen simultaneously. H$_2$O from the electrolyte solution starts the anodization process and creates a TiO$_2$ layer. Simultaneously, pits form on
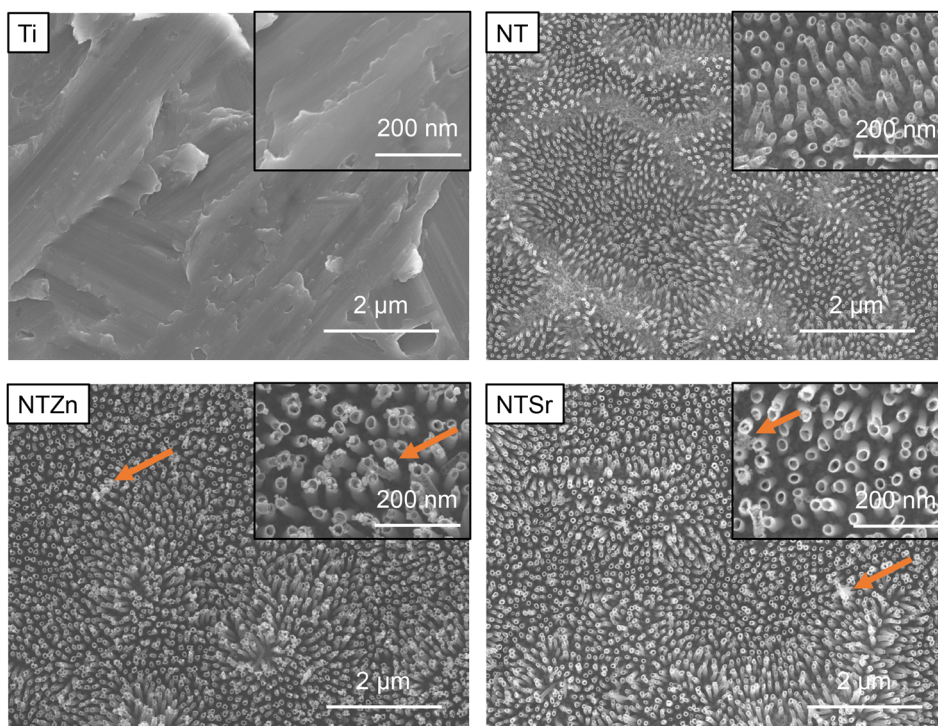
Fig. 1 SEM images of different surfaces.

this TiO$_2$ layer due to the electric field dissolution of oxide layer. In those pits, the F$^-$ from HF starts etching the oxide layer to form tubular nanotube structures.[25] As shown in SEM images in Fig. 1, the tube-like structures were evenly distributed on the surfaces. The nanotubes were around 80–100 nm long with a 30–50 nm diameter. During the hydrothermal doping process, Zn ions from the zinc acetate solution forms ZnO which get embedded into the TiO$_2$ nanotubes. The NTZn surfaces had crystal-like structures (pointed by arrows in Fig. 1) on top of nanotubes which were Zn crystals deposits from the hydrothermal treatment (confirmed by EDS, described later). The Zn crystals were found to be randomly distributed throughout the surface with certain areas having higher concentration of crystals.[21] Further, SEM images revealed that NTSr surfaces had larger rod-shaped crystals (pointed by arrows in Fig. 1). These crystals were significantly larger in size compared to the Zn crystals on the NTZn surface. During the Sr doping by hydrothermal treatment, Sr ions from the strontium acetate octahydrate form SrTiO$_3$ (confirmed by XRD spectra analysis, described later) with TiO$_2$ that results into large crystals. A small amount of SrF$_2$ is also formed during this stage by the reaction between residual F$^-$ ions from anodization and Sr ions (confirmed by XPS, described later). The formed crystals were mostly evenly distributed throughout the surface. Like the NTZn surface, certain areas on NTSr surfaces had higher concentration of these crystals.

Uniform distribution of Zn and Sr on the surfaces is important to ensure a consistent surface for better osseointegration. Energy dispersive X-ray spectroscopy (EDS) maps were col-

lected to understand the Zn and Sr distribution on different surfaces. The EDS maps can also confirm whether the crystals observed in SEM were Zn and Sr or not. EDS maps presented in Fig. 2 showed the Zn and Sr distributions. The results confirmed that observed crystals in SEM images were indeed Zn and Sr (confirmed by the purple-colored Zn and yellow-colored Sr maps). The images also indicated that the ions were evenly distributed throughout the surfaces with some area of higher concentrations. These results support the findings from SEM images.

Surface chemistry analysis is an important aspect to understand the successful chemical modification on different surfaces. To understand the surface chemistry, XPS spectra were collected for all the surfaces (Fig. 3). Metal oxides such as TiO$_2$ is formed on metals as a natural process when the metal surface is in contact with atmospheric oxygen. The anodization process helps to enhance this oxide formation while the presence of fluoride (F$^-$) ion in the electrolyte etches the oxide layer to form nanotubes. So, the surface chemistry of the NT should not be drastically different than Ti, which was confirmed from the XPS spectra (Fig. 3). However, after Zn and Sr doping, new peaks were formed on the surfaces. Zn 2p peaks were identified at 1016 eV and 1021 eV binding energy, which confirmed the presence of Zn ions on the NTZn surface. On the other hand, Sr 3s and Sr 3p peaks were identified at 357 eV and 268 eV on the NTSr surface, confirming the presence of Sr on this surface. NTSr also had an additional peak at 133 eV (Sr 3d). This peak indicates the presence of SrF$_2$ which formed during the hydrothermal process. It is possible that some

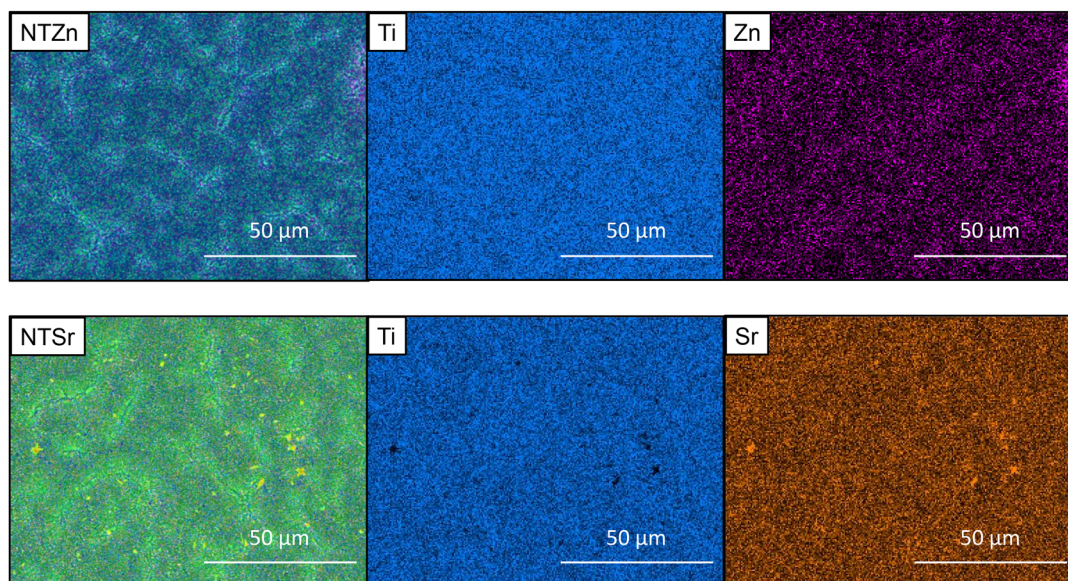**Fig. 2** EDS maps of Ti, Zn and Sr on NTZn and NTSr surfaces.
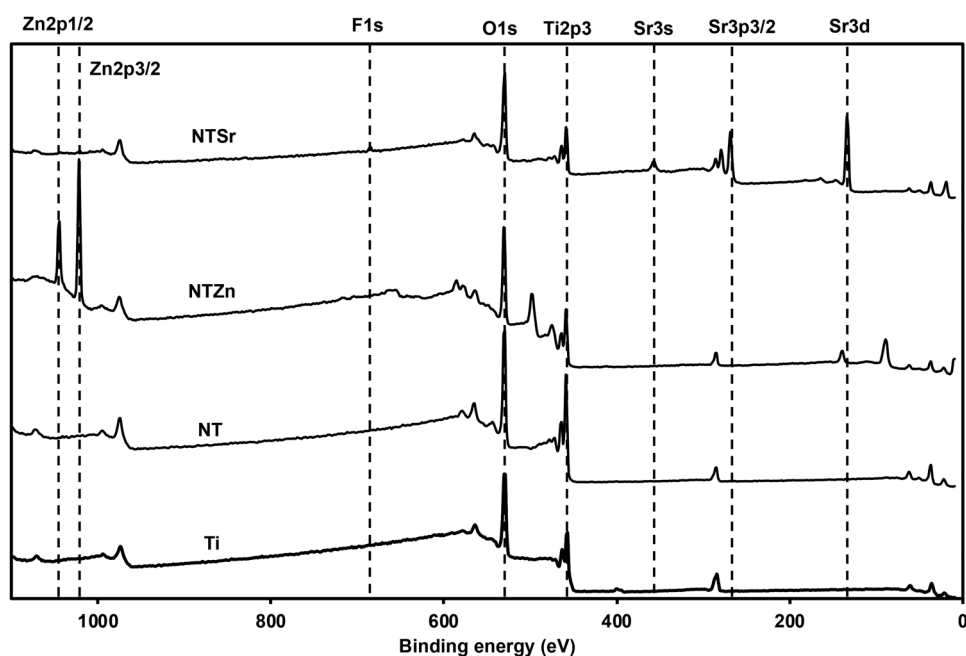

Fig. 3 XPS spectra of different surfaces.

residual F^- ions might have remained on the surface after anodization and interreacted with the Sr ions during the hydrothermal process to form SrF_2. Since the amount of F^- was significantly less in the final NTSr surface, it should not possess any cytotoxicity towards human cells (confirmed by cytotoxicity test, described later).

Relative atomic weight percentage (at%) of different elements on the surfaces was calculated from the XPS survey spectra (Table 1). The at% for Zn was 22% on NTZn, while Sr was 16% on NTSr. The Sr at% of was a bit lower compared to

Table 1 Elemental composition of different surfaces from XPS survey spectra. The compositions are expressed as relative atomic weight percentage (at%)

Surface	% Zn	% Sr	% F
Ti	0	0	0
NT	0	0	0
NT_{hyt}	22	0	0
NT_{Sr}	0	16.1	0.8

Zn probably due to the lower concentration of strontium acetate octahydrate during the hydrothermal process. These at% can be optimized by changing the concentrations of the acetates, temperature, and time used during the hydrothermal process. However, a thorough cytotoxicity analysis should follow because a higher Zn or Sr concentration can be toxic to the human cells. The presence of F on the NTSr surface was confirmed to be very low (0.8%).

Surface wettability is an important material property that can influence cell adhesion, proliferation, and differentiation to osteoblasts. Previous studies have suggested that a superhydrophilic surface can improve cell adhesion.[26,27] Other studies also suggest that superhydrophilic surfaces can reduce bacteria adhesion and proliferation, thus reducing the risk of bacterial infection owing to the surgical procedures of implant insertion in the host.[28] When the contact angle is less than 10°, then the surface is superhydrophilic. The static water contact angle of NT and NTSr was measured as 0°, confirming these surfaces were superhydrophilic (Fig. 4). The NTZn surface was hydrophilic since the contact angle was a little bit higher (17°) than NT and NTSr surfaces. Due to the presence of tubular structures on the NT surfaces, water molecules get trapped between the empty spaces of the tubes, creating a thin water layer on the surface that makes the surfaces superhydrophilic. However, when Zn crystals were deposited on the NT, they likely had disrupted the thin hydrophilic layer and reduced the hydrophilic properties. On the other hand, since the concentration of Sr was lower on the NTSr surface, the effect of the Sr crystals to disrupt the hydrophilic layer probably reduced, hence the difference in the contact angle.

Surface crystallinity affects the stem cell adhesion, growth, and differentiation.[29] Thus, determining crystalline phases of the modified Ti surfaces is important to understand the probability of the cell compatibility of these surfaces. As a metal, Ti creates a thin oxide layer of TiO_2 on its surface, which mostly constitutes of anatase phase (Fig. 5). During the anodization process, this thin TiO_2 layer was etched by the F^- ion and NT shapes were achieved. However, the NTs were amorphous in
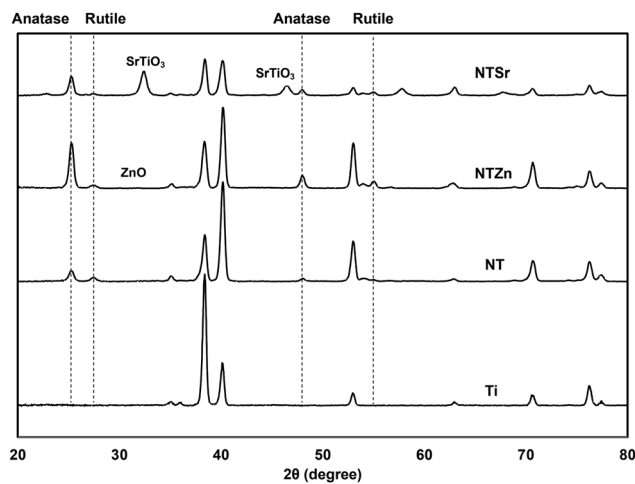

Fig. 5 XRD spectra of different surfaces.

this stage. So, to stabilize the structure for further applications, annealing was conducted at 530 °C which converted the amorphous regions to crystalline phases. In previous reports it was identified that when both anatase and rutile phases are present in the TiO_2 layer, cell spreading, and differentiation can improve.[29] Similarly, in this study, both anatase and rutile phases were observed on the NT surfaces at 2θ values of 25°, 48° and 27°, 55° respectively. The result aligned with the previously reported peaks for TiO_2.[30] NTSr had prominent $SrTiO_3$ peaks at 32.55° and 46.68° that confirmed the presence of Sr on the surface. On the other hand, NTZn had a very small ZnO peak at 31.72°.

Mechanical properties of a material surface deeply influence the bioactivity towards the stem cells. Besides, mechanical property analysis can also provide valuable information about the characteristics of the surface important for orthopedic implant applications where constant dynamic load is a factor. Since the surfaces used in this study have nanoscale characteristics, a traditional Instron Tester was deemed unable to identify key mechanical properties owing to the nanofeatures on these surfaces. For that reason, nanoindentation technique was applied to calculate surface hardness (H) and elastic modulus (E). All the NT surfaces (NT, NTZn, and NTSr) had lower H and E compared to the Ti surface as shown in Table 2. Since the nanotubes are flexible in nature, they probably deflected the nanoindenter and accommodated the applied force, resulting in a softer surface. These flexible and softer surfaces are imperative for the spreading, growth, and differen-
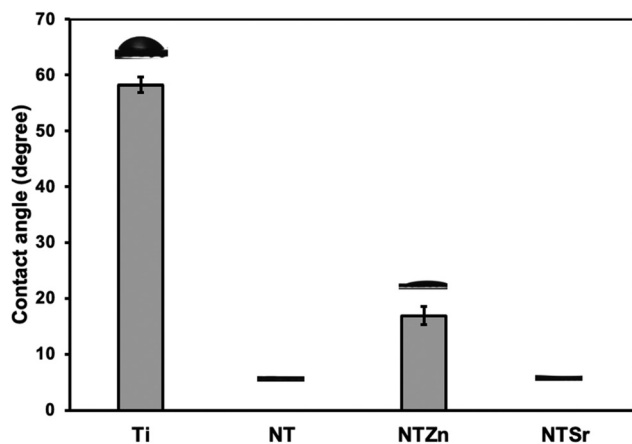

Fig. 4 Static water contact angle measurements of the surfaces.

Table 2 Nanoindentation hardness (H) and elastic modulus (E) values of different surfaces

Surface	Nanoindentation hardness (GPa)	Elastic modulus (GPa)
Ti	2.52 ± 0.35	138.41 ± 15.96
NT	0.51 ± 0.06	53.17 ± 3.93
NTZn	0.29 ± 0.02	45.19 ± 3.18
NTSr	0.25 ± 0.05	37.64 ± 4.58

tiation of stem cells to osteoblasts. Previous reports indicated that a softer surface could accommodate mechanical responses coming from the adhered cells which influences the specific phenotypic differentiation.[31] The elastic modulus and nanoindentation hardness of human trabecular bone is reported as 13.4 GPa and 0.47 GPa.[32] The NT surfaces, especially the NTSr surface has the closest values, thus resembling the mechanical properties of human trabecular bone. Moreover, since the NTs are flexible in nature, they can accommodate the mechanoresponse of ADSCs and help to improve the differentiation these cells to osteoblasts.

Stability of doped Zn and Sr is a crucial for long term effectiveness of implant surfaces. Further, inability of the surfaces to release these important signaling elements to the surrounding environment will reduce the efficacy of the implants. For that reason, stability of the modified surfaces was evaluated by analyzing XPS survey spectra after 0 and 28 days of incubation with DI Water. At day 0, atomic weight% of Zn on NTZn surface was around 23% (Fig. 6). However, it reduced to approximately 5% after 28 days. This indicates that significant amount of Zn was released in the surrounding DI water. A similar trend was observed for the Sr on NTSr surface. At day 0, the atomic weight% of Sr was around 22%, however it was reduced to 10% after 28 days. These results strongly indicate that the NTZn and NTSr surfaces release Zn and Sr respectively in the surrounding environment that may enhance signaling effects for cell differentiation.

Since Zn and Sr surfaces are released from the modified surfaces, it is important to evaluate the cytotoxicity of these surfaces. This is because Zn and Sr overdose can cause toxicity towards surrounding cell and tissue.[33,34] To evaluate cytotoxicity, lactate dehydrogenase (LDH) based indicator assay was used since damaged mammalian cells release LDH enzyme into the surrounding cell media.[35] Two controls were used to evaluate the cytotoxicity of the surfaces: spontaneous LDH release (SR) and maximum LDH release (MR). SR absorbance values were calculated by culturing the ADSCs without any surface, whereas MR values were calculated by damaging all the cultured cells using a 10× lysis buffer. Therefore, MR provided the maximum amount of LDH released from the ADSCs in a culture which indicate the maximum cytotoxicity. On the other hand, SR values indicated no cytotoxicity because no ADSCs were damaged. All the modified surfaces in this study had absorbance values comparable to SR and significantly lower than MR (Fig. 7), confirming that the surfaces do not exhibit any apparent cytotoxicity towards ADSCs.

Orthopedic implants are extrinsic materials to the host. So, an immediate immune response occurs when an orthopedic implant is placed inside the host. However, if the surface of the implant resembles the host body chemistry, then the immune response slows down and the implant gets acclimated to the host environment which helps in bone healing. For a successful bone healing process, cell adhesion, spread, and proliferation to the implant surface is necessary. Enhanced cell adhesion and proliferation on the implant surface can result in better osteogenic differentiation in later stage which influence better bone regeneration and healing process. ADSCs were cultured with the surfaces for 4 and 7 days to evaluate cell adhesion and proliferation. The fluorescence microscopy images (Fig. 8) showed that all the surfaces had successful cell adhesion after the culture period. However, a closer look reveals that the NTSr surfaces had more cell adhesion compared to the other surfaces. Also, adhered cells on the NT surfaces (NT, NTZn, and NTSr) covered more area compared to the Ti, indicating better cell proliferation.

The number of adhered cells were counted from the fluorescence microscopy images. It was observed that at day 4, all the modified surfaces (NT, NTZn, and NTSr) had higher cell adhesion compared to the Ti surface (Fig. 9). The result aligned with the fluorescence images and indicated that the Zn and Sr doping on surfaces could successfully facilitate higher cell adhesion. At day 7, the Ti surface however caught up to the modified surfaces. The reason behind this can be explained from the surface area and cell proliferation capa-
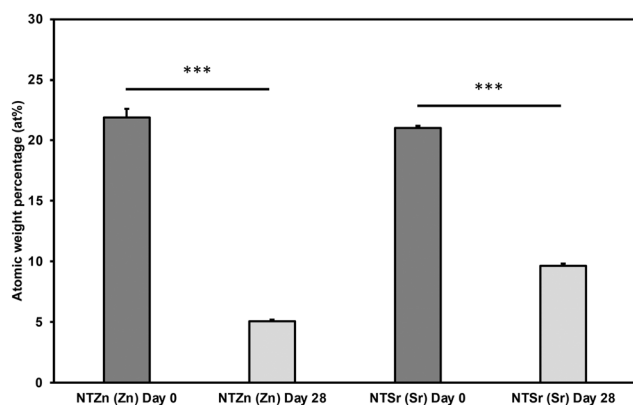

Fig. 6 Atomic weight percentages (at%) of Zn and Sr on the surfaces after 0 and 28 days of incubation with DI water. Statistical significances (*p*-value) were represented as *** *p* < 0.001.
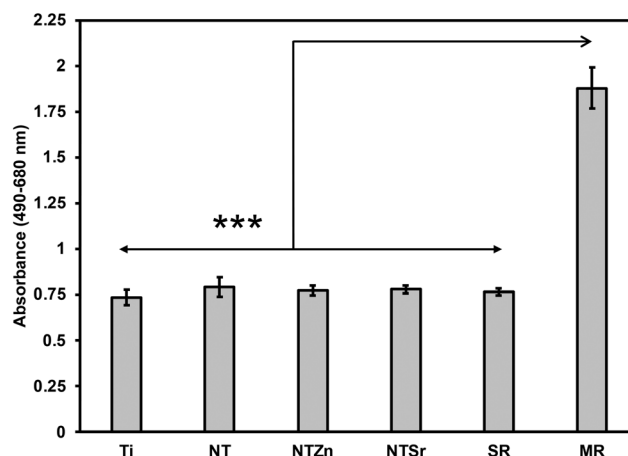

Fig. 7 Cytotoxicity evaluation of different surfaces. SR = spontaneous LDH release, MR = maximum LDH release. Statistical significances (*p*-value) were represented as *** *p* < 0.001.
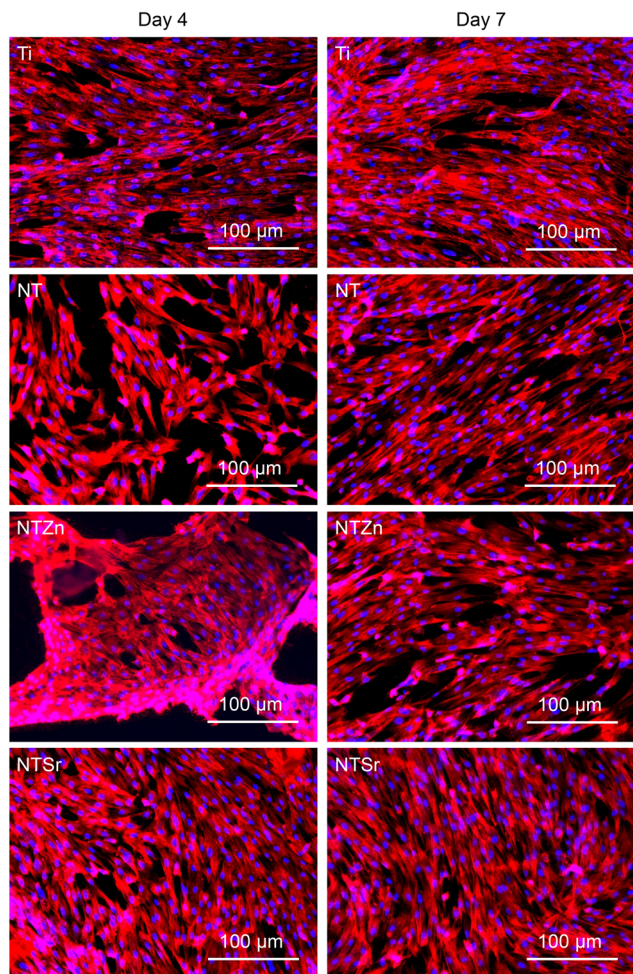
Fig. 8 Fluorescence microscope images of the surfaces after 4 and 7 days of incubation with ADSCs.
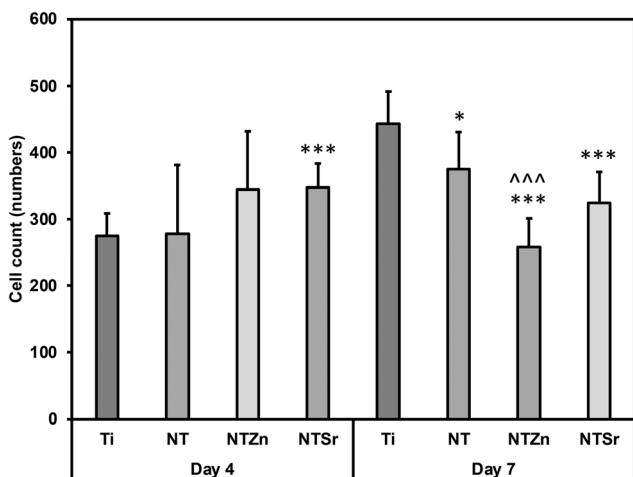

Fig. 9 ADSC count on each surface after 4 and 7 days of incubation calculated from the fluorescence images. Statistical significances (p-value) were represented as * $p < 0.05$ and *** $p < 0.001$ when compared to Ti, and ^^^ $p < 0.001$ when compared to NT.

bility. Since NTs provide better anchoring points for the cells to adhere to the surface, they spread better on the surfaces overtime which may also help in better osteogenic differentiation. After 7 days of incubation, adhered cells captured almost all the surface area and due to more spreading of cells on the NT surfaces, the number of cells seemed lower in calculation.

To understand the cell morphology on the surfaces, SEM images were collected after 4 and 7 days of incubation (Fig. 10). The relatively dark areas on the SEM images represents the adhered cells. The adhered cells on the Ti surfaces had very thin morphology compared to the NT surfaces. Interestingly, the adhered cells on the NTZn and NTSr surfaces had long extensions which may have resulted from better anchorage provided by the nanotube architecture. These extensions also facilitated better cell communication and spreading which can influence osteoblastic differentiation when suitable environment is provided. After 7 days of incubation, all the surfaces were mostly covered by the cells. But the NTZn and NTSr surfaces still showed the extension like structures which matched the results observed on Day 4.

To promote cell differentiation on different surfaces, differentiation media was introduced to the cells after 7 days of
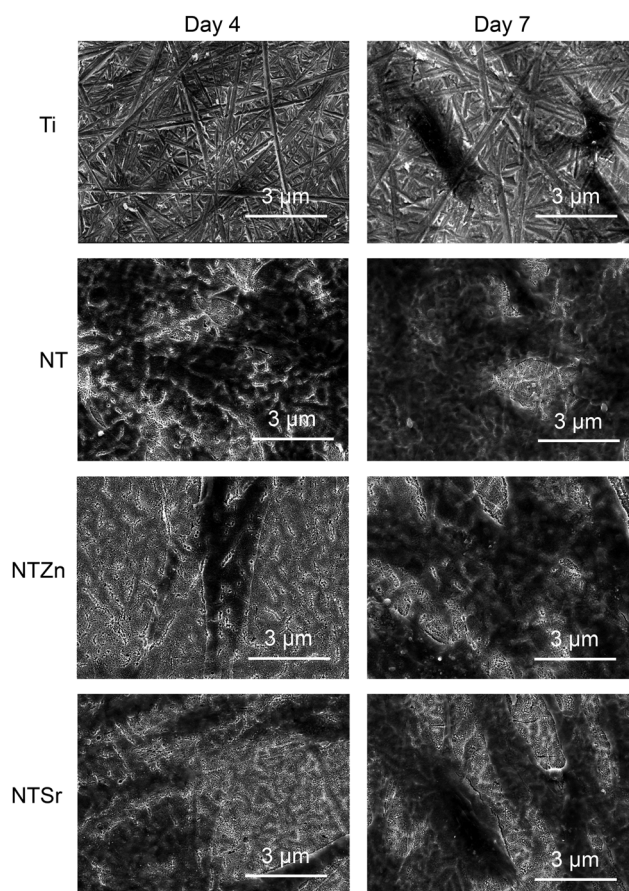

Fig. 10 SEM images of the surfaces after 4 and 7 days of incubation with ADSCs.

culture on all surfaces. Then, after 1 and 3 weeks of culture in differentiation media, several biochemical assays were used to understand the cell differentiation potential. Firstly, alkaline phosphatase (ALP) activity of the differentiated cells was evaluated (Fig. 11). ALP activity is considered as an early indication of osteoblast differentiation since the ALP activity peaks just before bone mineralization begins.[36] Hydroxyapatite is the mineral phase of bone and increased ALP activity indicates increased level of inorganic phosphate, which is a major component of hydroxyapatite.[4,36] All the surfaces had similar level of ALP activity after 1 week (Fig. 11). However, the average ALP activity was higher for the NT surfaces compared to the Ti surface. After week 3, NTZn had the highest ALP activity of all the surfaces. NTSr had lower ALP activity compared to the Ti surface which indicated that the ALP activity reduced because mineralization had already begun, which aligns with the early mineralization activity by NTSr confirmed by SEM images (discussed later). From the results, it was evident that ALP activity was higher in modified surfaces which is a good indication of ADSC differentiation on these surfaces.

Then osteocalcin expression from the differentiated ADSCs was evaluated. Osteocalcin is a hormone released by matured osteoblasts and is a good indication of differentiation into osteoblasts.[37] Immunofluorescence images were utilized to understand the osteocalcin expression as shown in Fig. 12. The green areas are expressed osteocalcin from the differentiated ADSCs. After 1 week, osteocalcin expressed from Ti and NT surfaces were very low. However, osteocalcin released from both NTZn and NTSr were higher than the Ti surface, indicating a faster ADSC differentiation to osteoblasts on these surfaces.

Then quantitative analysis was conducted by calculating the osteocalcin area coverage on the images normalized by the attached cells (Fig. 13). NTZn and NTSr surfaces had significantly higher osteocalcin expression after 1 week, which is a strong indication of ADSC differentiation to osteoblasts. After 3 weeks, all the NT surfaces expressed significantly higher osteocalcin than unmodified Ti surface. NTSr surface had the
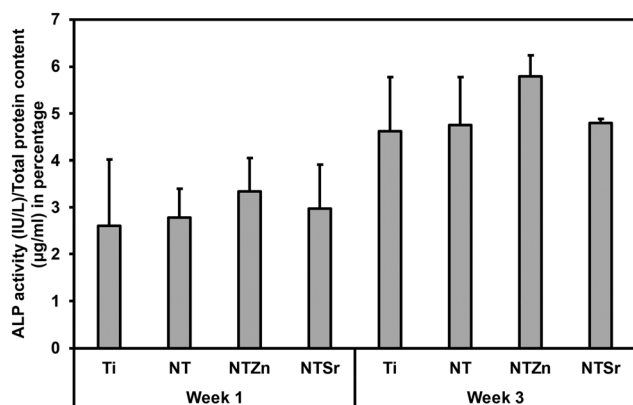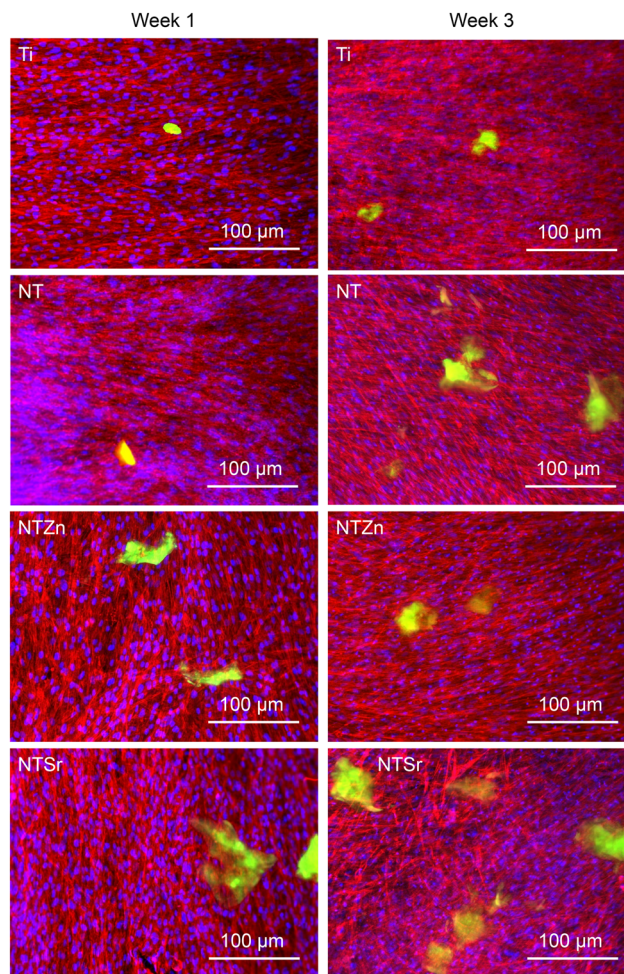

Fig. 12 Immunofluorescence microscopic images of the surfaces after 1 and 3 weeks of culturing ADSCs with differentiation media. The green color represents osteocalcin expression by the differentiated ADSCs.
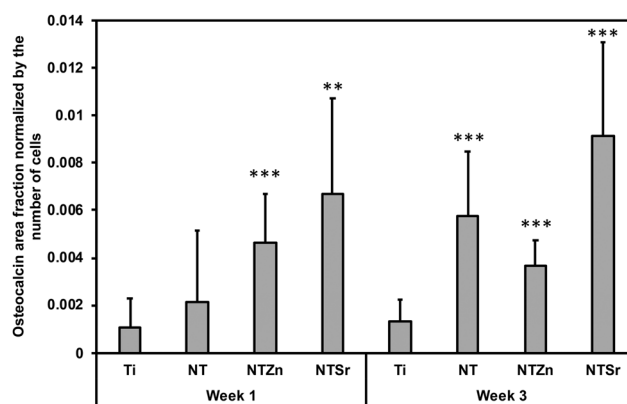

Fig. 13 Osteocalcin area fraction normalized by the number of adhered ADSCs to the surfaces. Statistical significances (p-value) were represented as ** $p < 0.01$ and *** $p < 0.001$.

Fig. 11 ALP activity of differentiated ADSCs on different surfaces after 1 and 3 weeks, normalized by the total protein content.

significantly higher osteocalcin expression among the modified surfaces. From the result, it is evident that modified surfaces, especially NTSr help in better ADSC differentiation com-
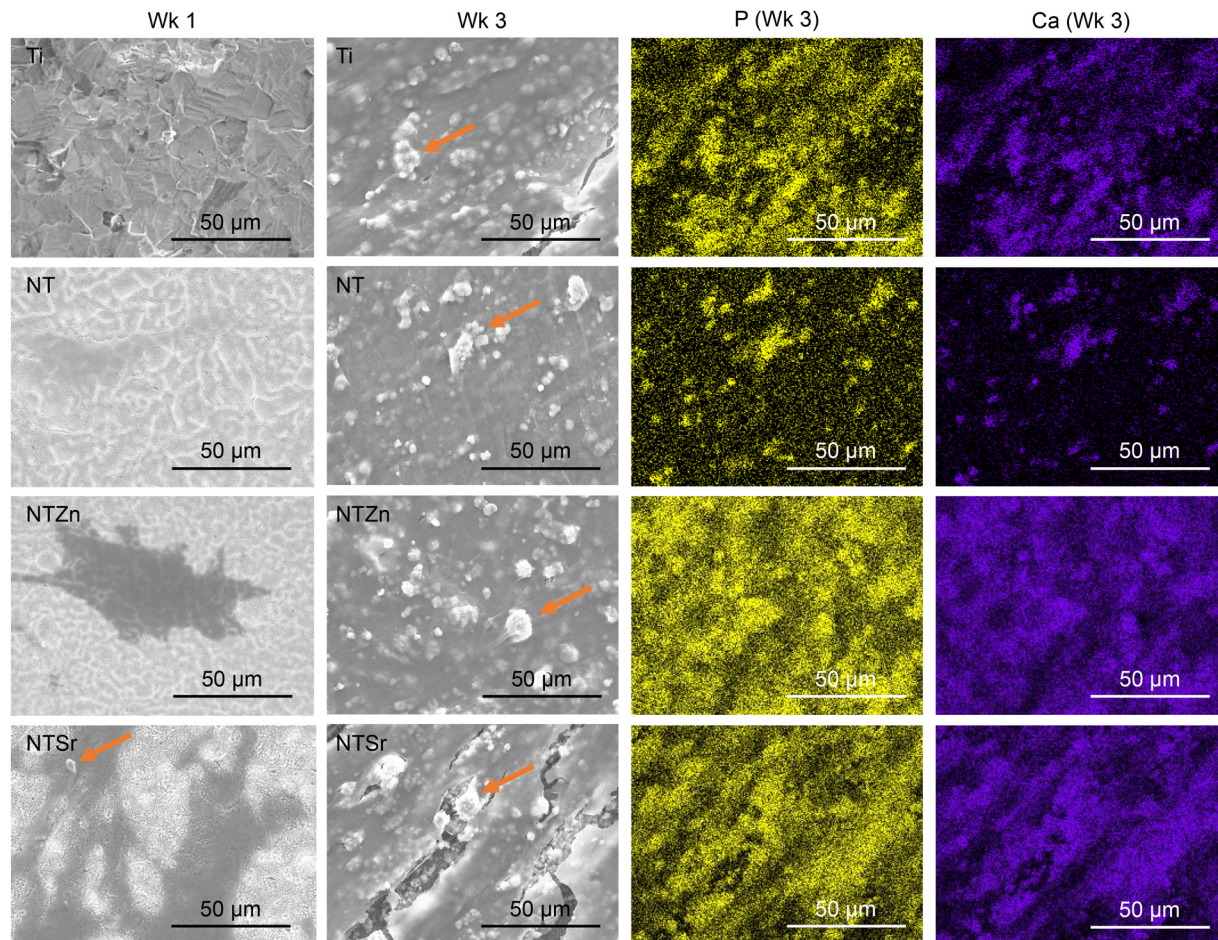
Fig. 14 SEM images and EDS maps of the surfaces after introducing osteoblast differentiation to ADSCs. Arrow marks show the HA crystal deposition on the surfaces.

pared to unmodified Ti surface which may have resulted from the better ADSC adhesion and spreading.

Mineralization initiates when osteoblasts start producing hydroxyapatite (HA) that is composed of calcium and phosphorus.[37] Released ALP from the osteoblasts reacts with the contents from differentiation media resulting in HA crystals that are deposited on the surfaces as minerals.[37] These crystals are easily visible by SEM images (Fig. 14). Additionally, EDS mapping is a crucial tool to confirm the contents of HA crystals. After 1 week of ADSC culturing with the differentiation media, no surfaces had any HA crystal deposition except for NTSr (Fig. 14, arrow marked). This is another strong indication of early ADSC differentiation and mineralization on the NTSr surface confirming the findings in ALP activity. After 3 weeks, all the surfaces had increased amount of crystal deposition (white circular shapes, arrow marked in Fig. 14). However, the modified surfaces showed enhanced mineral deposition compared to the pure Ti surface, confirming improved ADSC differentiation and new bone matrix formation by the modified surfaces. To confirm the elemental composition of these crystals, EDS maps were collected (Fig. 14). It was observed that all the minerals were composed of calcium (Ca) and phosphorus (P),

which confirmed the mineralization of ADSCs resulting from differentiation of these cells into osteoblasts. From the Ca and P maps, it was also identified that the amount of Ca and P was much higher than Ti and NT surfaces, indicating a strong influence of Zn and Sr on the ADSC differentiation.

Conclusion

Nanosurface modification of titanium orthopedic implants have promising implications to improve their performance. In this work, TiO_2 nanotube (NT) arrays were fabricated on pure titanium (Ti) and doped with important signaling elements such as zinc (Zn) and strontium (Sr). Differences in surface morphology were identified from the SEM images. Both the NTZn and NTSr surfaces had crystal like structures but the shape and size of these crystals were different. EDS maps confirmed an even distribution of the doped elements with regions of high concentration. XPS spectra confirmed successful doping of the Zn and Sr along with their release profile over a 28-day period. XRD analysis confirmed the presence of rutile and anatase phases on the modified surfaces that can

help in cell compatibility. Nanoindentation technique was utilized to evaluate indentation hardness and elastic modulus of the modified surfaces. It was observed that the modified surfaces were flexible in nature that can help in accommodating dynamic response coming from the cells during cell adhesion, proliferation, and growth. Studies with ADSCs revealed enhanced cell adhesion, proliferation, and growth properties of the modified surfaces, especially the NTSr, confirming the efficacy of signaling element. The differentiation assays revealed that NTSr performed significantly better to start early and faster differentiation of the adhered ADSCs into osteoblasts. This study provided an interesting approach to fabricate titanium orthopedic implants with NTs and important signaling elements like Zn and Sr that holds potential to effectively improve the performance of orthopedic implants by improving osseointegration.

Conflicts of interest

There are no conflicts to declare.

Acknowledgements

References

1 S. H. Ralston, Bone structure and metabolism, *Medicine*, 2013, **41**(10), 581–585, DOI: **10.1016/j.mpmed.2013.07.007**.

2 T. Albrektsson and C. Johansson, Osteoinduction, osteoconduction and osseointegration, *Eur. Spine J.*, 2001, **10**(Suppl 2), S96–S101, DOI: **10.1007/s005860100282**.

3 M. T. Frassica, S. K. Jones, P. Diaz-Rodriguez, M. S. Hahn and M. A. Grunlan, Incorporation of a silicon-based polymer to PEG-DA templated hydrogel scaffolds for bioactivity and osteoinductivity, *Acta Biomater.*, 2019, **99**, 100–109, DOI: **10.1016/j.actbio.2019.09.018**.

4 R. M. Sabino, G. Mondini, M. J. Kipper, A. F. Martins and K. C. Popat, Tanfloc/heparin polyelectrolyte multilayers improve osteogenic differentiation of adipose-derived stem cells on titania nanotube surfaces, *Carbohydr. Polym.*, 2021, **251**, 117079, DOI: **10.1016/j.carbpol.2020.117079**.

5 E. Gibon, D. F. Amanatullah, F. Loi, J. Pajarinen, A. Nabeshima, Z. Yao, M. Hamadouche and S. B. Goodman, The biological response to orthopaedic implants for joint replacement: Part I: Metals, *J. Biomed. Mater. Res., Part B*, 2017, **105**(7), 2162–2173, DOI: **10.1002/jbm.b.33734**.

6 B. S. Smith, S. Yoriya, L. Grissom, C. A. Grimes and K. C. Popat, Hemocompatibility of titania nanotube arrays, *J. Biomed. Mater. Res., Part A*, 2010, **95**(2), 350–360, DOI: **10.1002/jbm.a.32853**.

7 J. C. Souza, M. B. Sordi, M. Kanazawa, S. Ravindran, B. Henriques, F. S. Silva, C. Aparicio and L. F. Cooper, Nano-scale modification of titanium implant surfaces to enhance osseointegration, *Acta Biomater.*, 2019, **94**, 112–131, DOI: **10.1016/j.actbio.2019.05.045**.

8 V. K. Manivasagam, R. M. Sabino, P. Kantam and K. C. Popat, Surface modification strategies to improve titanium hemocompatibility: A comprehensive review, *Mater. Adv.*, 2021, **2**(18), 5824–5842, DOI: **10.1039/D1MA00367D**.

9 K. C. Popat, L. Leoni, C. A. Grimes and T. A. Desai, Influence of engineered titania nanotubular surfaces on bone cells, *Biomaterials*, 2007, **28**(21), 3188–3197, DOI: **10.1016/j.biomaterials.2007.03.020**.

10 B. S. Smith, P. Capellato, S. Kelley, M. Gonzalez-Juarrero and K. C. Popat, Reduced in vitro immune response on titania nanotube arrays compared to titanium surface, *Biomater. Sci.*, 2013, **1**(3), 322–332, DOI: **10.1039/C2BM00079B**.

11 J. Chen, X. Shi, Y. Zhu, Y. Chen, M. Gao, H. Gao, L. Liu, L. Wang, C. Mao and Y. Wang, On-demand storage and release of antimicrobial peptides using Pandora's box-like nanotubes gated with a bacterial infection-responsive polymer, *Theranostics*, 2020, **10**(1), 109, DOI: **10.7150/thno.38388**.

12 D. Chen, L. C. Waite and W. M. Pierce, In vitro effects of zinc on markers of bone formation, *Biol. Trace Elem. Res.*, 1999, **68**, 225–234, DOI: **10.1007/BF02783905**.

13 A. Bian, Y. Sun, J. Guan, L. Xie, H. Yang, P. Han, H. Lin, H. Qiao, X. Zhang and Y. Huang, Dopamine-mediated copper-loaded ZnTiO3 antimicrobial coating with immunomodulatory properties effectively enhances vascularised osteogenesis on titanium implants, *J. Ind. Eng. Chem.*, 2024, **135**, 94–109, DOI: **10.1016/j.jiec.2024.01.022**.

14 K. Huo, X. Zhang, H. Wang, L. Zhao, X. Liu and P. K. Chu, Osteogenic activity and antibacterial effects on titanium surfaces modified with Zn-incorporated nanotube arrays, *Biomaterials*, 2013, **34**(13), 3467–3478, DOI: **10.1016/j.biomaterials.2013.01.071**.

15 J. Ye, B. Li, M. Li, Y. Zheng, S. Wu and Y. Han, ROS induced bactericidal activity of amorphous Zn-doped titanium oxide coatings and enhanced osseointegration in bacteria-infected rat tibias, *Acta Biomater.*, 2020, **107**, 313–324, DOI: **10.1016/j.actbio.2020.02.036**.

16 Y. Li, W. Xiong, C. Zhang, B. Gao, H. Guan, H. Cheng, J. Fu and F. Li, Enhanced osseointegration and antibacterial action of zinc–loaded titania–nanotube–coated titanium substrates: In vitro and in vivo studies, *J. Biomed. Mater. Res., Part A*, 2014, **102**(11), 3939–3950, DOI: **10.1002/jbm.a.35060**.

17 J. Shi, Y. Li, Y. Gu, S. Qiao, X. Zhang and H. Lai, Effect of titanium implants with strontium incorporation on bone apposition in animal models: A systematic review and

meta-analysis, *Sci. Rep.*, 2017, **7**(1), 15563, DOI: **10.1038/s41598-017-15488-1**.

18 F. Jia, D. Xu, Y. Sun, W. Jiang, H. Yang, A. Bian, Y. Liu, K. Liu, S. Zhang, Y. Wang and H. Qiao, Strontium-calcium doped titanium dioxide nanotubes loaded with GL13K for promotion of antibacterial activity, anti-Inflammation, and vascularized bone regeneration, *Ceram. Int.*, 2023, **49**(22), 35703–35721, DOI: **10.1016/j.ceramint.2023.08.250**.

19 C. Gao, C. Li, C. Wang, Y. Qin, Z. Wang, F. Yang, H. Liu, F. Chang and J. Wang, Advances in the induction of osteogenesis by zinc surface modification based on titanium alloy substrates for medical implants, *J. Alloys Compd.*, 2017, **726**, 1072–1084, DOI: **10.1016/j.jallcom.2017.08.078**.

20 A. Bhattacharjee, E. Goodall, B. L. Pereira, P. Soares and K. C. Popat, Zinc (Zn) Doping by Hydrothermal and Alkaline Heat-Treatment Methods on Titania Nanotube Arrays for Enhanced Antibacterial Activity, *Nanomaterials*, 2023, **13**(10), 1606, DOI: **10.3390/nano13101606**.

21 W. Tsuji, J. P. Rubin and K. G. Marra, Adipose-derived stem cells: Implications in tissue regeneration, *World J. Stem Cells*, 2014, **6**(3), 312, DOI: **10.4252/wjsc.v6.i3.312**.

22 L. Le Guehennec, M. A. Lopez-Heredia, B. Enkel, P. Weiss, Y. Amouriq and P. Layrolle, Osteoblastic cell behaviour on different titanium implant surfaces, *Acta Biomater.*, 2008, **4**(3), 535–543, DOI: **10.1016/j.actbio.2007.12.002**.

23 A. Zareidoost, M. Yousefpour, B. Ghaseme and A. Amanzadeh, The relationship of surface roughness and cell response of chemical surface modification of titanium, *J. Mater. Sci.: Mater. Med.*, 2012, **23**, 1479–1488, DOI: **10.1007/s10856-012-4611-9**.

24 H. Chouirfa, H. Bouloussa, V. Migonney and C. Falentin-Daudré, Review of titanium surface modification techniques and coatings for antibacterial applications, *Acta Biomater.*, 2019, **83**, 37–54, DOI: **10.1016/j.actbio.2018.10.036**.

25 P. Benjwal and K. K. Kar, One-step synthesis of Zn doped titania nanotubes and investigation of their visible photocatalytic activity, *Mater. Chem. Phys.*, 2015, **160**, 279–288, DOI: **10.1016/j.matchemphys.2015.04.038**.

26 J. Meng, G. Yang, L. Liu, Y. Song, L. Jiang and S. Wang, Cell adhesive spectra along surface wettability gradient from superhydrophilicity to superhydrophobicity, *Sci. China: Chem.*, 2017, **60**, 614–620, DOI: **10.1007/s11426-016-9031-8**.

27 H. Fan and Z. Guo, Bioinspired surfaces with wettability: biomolecule adhesion behaviors, *Biomater. Sci.*, 2020, **8**(6), 1502–1535, DOI: **10.1039/C9BM01729A**.

28 X. Q. Dou, D. Zhang, C. Feng and L. Jiang, Bioinspired hierarchical surface structures with tunable wettability for regulating bacteria adhesion, *ACS Nano*, 2015, **9**(11), 10664–10672, DOI: **10.1021/acsnano.5b04231**.

29 G. Wang, J. Li, K. Lv, W. Zhang, X. Ding, G. Yang, X. Liu and X. Jiang, Surface thermal oxidation on titanium implants to enhance osteogenic activity and in vivo osseointegration, *Sci. Rep.*, 2016, **6**(1), 31769, DOI: **10.1038/srep31769**.

30 K. Thamaphat, P. Limsuwan and B. Ngotawornchai, Phase characterization of TiO2 powder by XRD and TEM, *J. Agric. Nat. Resour.*, 2008, **42**(5), 357–361, **https://li01.tci-thaijo.org/index.php/anres/article/view/244620**.

31 Q. Sun, Y. Hou, Z. Chu and Q. Wei, Soft overcomes the hard: Flexible materials adapt to cell adhesion to promote cell mechanotransduction, *Bioact. Mater.*, 2022, **10**, 397–404, DOI: **10.1016/j.bioactmat.2021.08.026**.

32 J. Y. Rho, T. Y. Tsui and G. M. Pharr, Elastic properties of human cortical and trabecular lamellar bone measured by nanoindentation, *Biomaterials*, 1997, **18**(20), 1325–1330, DOI: **10.1016/S0142-9612(97)00073-2**.

33 F. Piao, K. Yokoyama, N. Ma and T. Yamauchi, Subacute toxic effects of zinc on various tissues and organs of rats, *Toxicol. Lett.*, 2003, **145**(1), 28–35, DOI: **10.1016/S0378-4274(03)00261-3**.

34 S. P. Nielsen, The biological role of strontium, *Bone*, 2004, **35**(3), 583–588, DOI: **10.1016/j.bone.2004.04.026**.

35 N. Uchide, K. Ohyama, T. Bessho and H. Toyoda, Lactate dehydrogenase leakage as a marker for apoptotic cell degradation induced by influenza virus infection in human fetal membrane cells, *Intervirology*, 2009, **52**(3), 164–173, DOI: **10.1159/000224644**.

36 K. Cowden, M. F. Dias-Netipanyj and K. C. Popat, Effects of titania nanotube surfaces on osteogenic differentiation of human adipose-derived stem cells, *Nanomedicine*, 2019, **17**, 380–390, DOI: **10.1016/j.nano.2019.01.008**.

37 S. C. Moser and B. C. van der Eerden, Osteocalcin—A versatile bone-derived hormone, *Front. Endocrinol.*, 2019, **9**, 794, DOI: **10.3389/fendo.2018.00794**.